Available online at www.sciencedirect.com
SCIENCE DIRECT®
Applied Surface Science 228 (2004) 365–372
applied surface science
www.elsevier.com/locate/apsusc

Nanomechanical properties of TiC, TiN and TiCN thin films using scanning probe microscopy and nanoindentation

Te-Hua Fang[a,*], Sheng-Rui Jian[b], Der-San Chuu[b]

[a]Department of Mechanical Engineering, Southern Taiwan University of Technology, Tainan 710, Taiwan, ROC
[b]Institute and Department of Electrophysics, National Chiao Tung University, Hsinchu 300, Taiwan, ROC

Received 11 December 2002; received in revised form 27 April 2003; accepted 13 January 2004

Abstract

TiC, TiN and TiCN thin films deposited on silicon (1 0 0) substrates using plasma enhanced chemical vapor deposition (PECVD) was investigated by scanning probe microscopy (SPM) and nanoindentation techniques. Results showed that the TiC film exhibits lower surface roughness and friction coefficient than the TiN and the TiCN films. Young's modulus and hardness both decreased as the indentation depth increased for all the films and the TiC film exhibited a higher hardness and Young's modulus. Additionally, the contact stress–strain relationships and fractal dimension were also analyzed.

Keywords: SPM; Nanoindentation; Young's modulus; Hardness; Friction; Fractal analysis

1. Introduction

Titanium carbide (TiC), titanium nitride (TiN) and titanium carbonitride [Ti(CN)] hard films are considered as high technology materials commonly used in micro-electrics, space technology, the aeroplane industry and the semiconductor technology due to their unique characteristics such as high hardness and Young's modulus, low friction, good corrosion resistance, good thermal conductivity, higher electric conductivity and higher melting temperatures [1–4].

Understanding the nanomechanical characteristics of a thin film's surface is significant today because the surface may be different for those bulk material surfaces that have had different treatments [5]. It is essential to study the mechanical and surface characteristics of these thin films and recognize how the relative parameters affect the material structures and properties for advanced applications. By means of the scanning probe microscopy (SPM), it is possible to find out the surface topography and nanofriction characteristics with a spatial resolution that is measured on the atomic scale. Nanoindentation is the most commonly used technique for quantifying thin film properties on a nanoscale such as Young's modulus and hardness [6–8].

There are many methods used to prepare TiC, TiN and TiCN films such as cathodic arc plasma deposition (CAPD) [9], magnetron sputtering [10], plasma assisted chemical vapor deposition (CVD) and metallic organic chemical vapor deposition (MOCVD) [11]. Each method has its relative advantages for certain applications. Among them, plasma enhanced chemical vapor deposition (PECVD) is a promising technique because of its superior plasma-species production rate

* Corresponding author. Fax: +886-6-2425092.
E-mail address: fang@mail.stut.edu.tw (T.-H. Fang).

0169-4332/$ – see front matter © 2004 Elsevier B.V. All rights reserved.
doi:10.1016/j.apsusc.2004.01.053

and ability to achieve uniformity during deposition on the film [12].

In this study, the surface analysis, nanofriction and nanomechanical characteristics of TiC, TiN and TiCN thin films deposited by PECVD were investigated by SPM and nanoindentation technique. Additionally, the contact stress–strain relationships and fractal dimension of the deposited films were studied.

2. Experiment details

TiC, TiN and TiCN thin films were prepared on silicon (1 0 0) substrates by the PECVD method with a rf bias applied to the substrates holder. A 13.56-MHz rf bias voltage was coupled to the substrate holder. The chamber was first evacuated to 0.01 Torr and then the gas mixture of ($TiCl_4$, N_2, CH_4, H_2) was introduced into chamber. The deposition parameters for the three kinds of films used are listed in Table 1. A square 20 μm × 20 μm area of the specimen surface was scanned at low resolution to get the optimum surface. If the surface was acceptable, the selected area was contracted to a 2 μm × 2 μm area for the friction and indentation experiments.

In addition, the average surface roughness, R_a, of the current sample was recorded for comparison with the test areas of subsequent samples in the experiment. Samples with comparable initial surface conditions were used throughout the entire experiments. The pre-scan procedures for nanoindentation, nanofriction and fractal analysis processes were the same.

The topographic properties and frictional properties of the thin films were analyzed by a SPM apparatus (Shimadzu SPM 9500-J2, Tokyo, Japan). A constant scan speed of 2 μm s^{-1} was used under a constant load of 100 nN. The atomic force microscopy (AFM) and friction force microscopy (FFM) imaging was performed simultaneously. AFM scanning uses only the two vertical quadrants to measure vertical deflection of the cantilever and thus the surface topography of the specimen. FFM scanning uses the other two horizontal quadrants to get the frictional force images of the sample's surfaces.

Table 1
Deposition conditions for TiC, TiN and TiCN thin films

Gas	$TiCl_4$, N_2, CH_4, H_2
Substrate	Si(1 0 0)
Deposition temperature (°C)	500
Pressure (Torr)	0.01
Power (W)	200

Nanomechanical properties such as Young's modulus and hardness of thin films were obtained by nanoindentation technique (Hysitron Triboscope, USA). Load controlled indentation testing followed a trapezoidal loading profile with a hold time of typically 10 s at peak load. Peak loads were ranged from 100 to 1000 μN at a loading rate of 10 μN s^{-1}. The diamond indenter was a Berkovich tip with a tip radius of 100 nm [6]. From the analyzed load–displacement curves, Young's modulus of measured films can be calculated as follow:

$$\frac{1}{E_r} = \frac{2\beta}{S}\sqrt{\frac{A_c}{\pi}} = \frac{1-\nu_m^2}{E_m} + \frac{1-\nu_i^2}{E_i} \quad (1)$$

where A_c, E_r, S and β are denoted as the actual contact area, the reduced elastic modulus for each indenter/specimen combination, the measured stiffness and a shape constant of 1.034 for the Berkovich tip, respectively. Where the subscript m and i are denoted as the film and the indenter tip, respectively, E is the Young's modulus and ν is Poisson's ratio. Indenter properties used in this study's calculations are $E_i = 1140$ GPa and $\nu_i = 0.07$, and assumed the Poisson's ratio to be $\nu_m = 0.17$ for TiC, $\nu_m = 0.19$ for TiN, and $\nu_m = 0.182$ for TiCN [13].

3. Results and discussion

3.1. Morphology and surface characteristics

The surface topographies of TiC, TiN and TiCN thin films deposited by PECVD are shown in Fig. 1a–c. It is known that island-like growths in the films are observed in all the AFM images. The lighter areas of AFM images represent those areas with a higher height.

The results of the surface roughness are shown in Table 2. It can be seen in Table 2, that R_a is defined as the mean value of the surface height relative to the center plane and rms is the root-mean-square roughness profile of the surface height within the scanned area and both have been used to explain

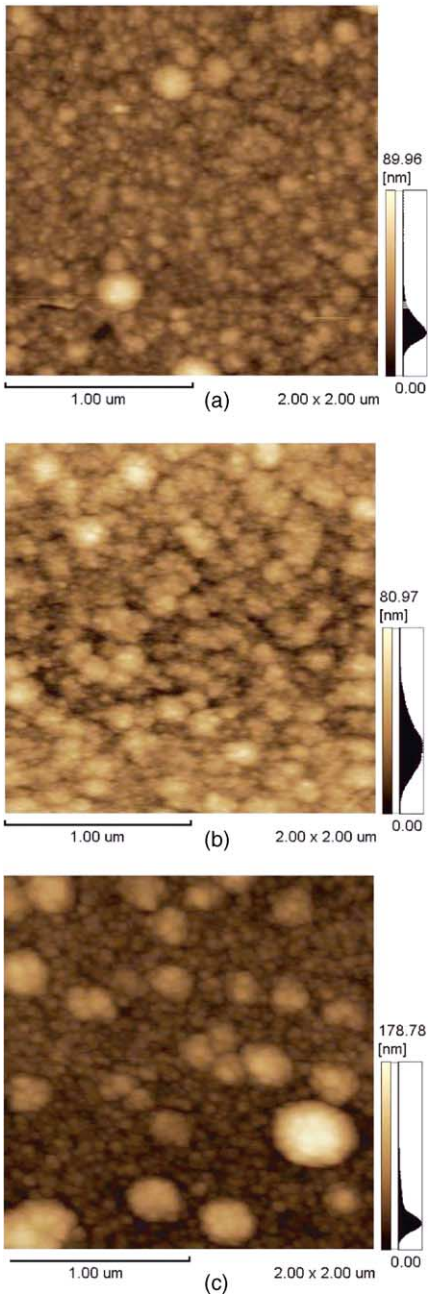

Fig. 1. AFM images of (a) TiC, (b) TiN, (c) TiCN thin films.

the surface morphology [14]. TiC film exhibits lower surface roughness than the others. The average roughness of TiC, TiN and TiCN films are 5.4, 8.9 and 16.1 nm, respectively.

Table 2
Surface roughness and friction coefficient of TiC, TiN and TiCN thin films

	TiC	TiN	TiCN
μ	0.28	0.33	0.40
R_a (nm)	5.4	8.9	16.1
rms (nm)	7.7	11.2	23.8

Fractal analysis has been used to determine the characteristics of surface irregularities on a variety of materials. It reveals the complexity of the surface morphology through fractal dimension analysis. It has been established in previous research that the roughness parameters based on conventional theories depend on the sampling interval of the particular measuring apparatus used [15].

In this study, the structure function method was adopted to analyze the fractal dimension of the deposited films [14]. The fractal dimension D_s is calculated from the least-square degeneration line on a log–log plot of structure function $S(\tau)$ versus a large vector τ [15]. All AFM images show self-affine structures. The fractal dimension determines the relative amount of the surface irregularities using different distance scales. The results of fractal analysis are shown in Fig. 2. The fractal dimension is approximate to 2 and exhibits a lower complicated geometry. Therefore, the higher the fractal dimension the rougher the surface

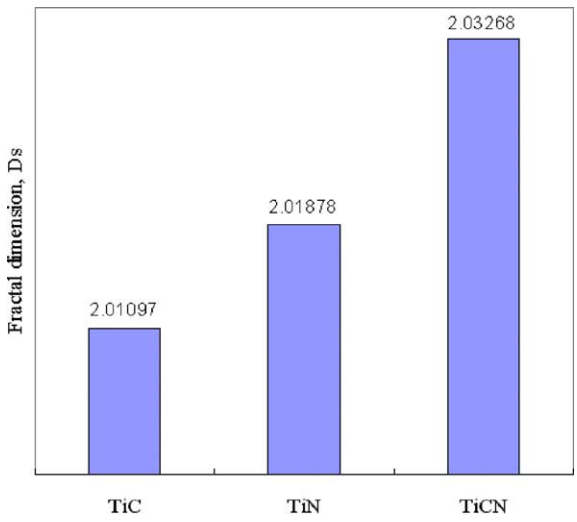

Fig. 2. Fractal dimension of TiC, TiN and TiCN thin films.

tends to be, i.e. TiC films have a smaller grain size and a larger surface roughness, on the contrary TiCN films own the opposite values.

3.2. Nanofriction tests

The frictional force images of TiC, TiN and TiCN thin films are shown in Fig. 3a–c. It can be compared with the surface morphology and frictional force images in Figs. 1 and 3. The light areas indicate a greater height in Fig. 1 and also indicate larger friction forces in Fig. 3. This indicates that there is a strong dependence between the surface asperity and the friction coefficient on a nanometer-scale. The friction coefficient (μ) defined as the average ratio of the friction to the normal load can be evaluated in Table 2. It can be seen that the TiC film exhibits lower friction coefficient and lower surface roughness than the TiN and the TiCN films. The results showed that the surface roughness R_a and rms are strongly affected by their structures. Further discussion of this subject can be found in the Ruan and Bhushan's studies [16–18], which investigated the influence of different surface asperity morphologies.

Fig. 4 shows the relationship of the friction force and various friction speeds under a constant applied load. The results showed that there was no direct effect on the friction forces as the friction speeds were increased. This phenomena maybe owing to the fact that the friction force represents, the ability of overcoming the bond energy, between the probe and the surface of samples at an atomic scale within every time step, there is no clear influence on the magnitude of the friction force when the scanning speed increases.

3.3. Nanoindentation tests

Fig. 5 illustrates that the load–unloading curves are obtained from a Berkovich diamond indenter at a load of 1000 μN. The penetration depth of TiC film was the lowest. It was clearly seen that the TiC film exhibited a higher hardness property than the TiN and the TiCN films at the same applied loads. The hardness for TiC, TiN and TiCN thin films are shown in Fig. 6. The hardnesses ranged from 20.56 to 23.64 GPa, 11.84 to 14.09 GPa and 8.24 to 11.02 GPa. The results show the hardness decreased slowly as the penetration depth

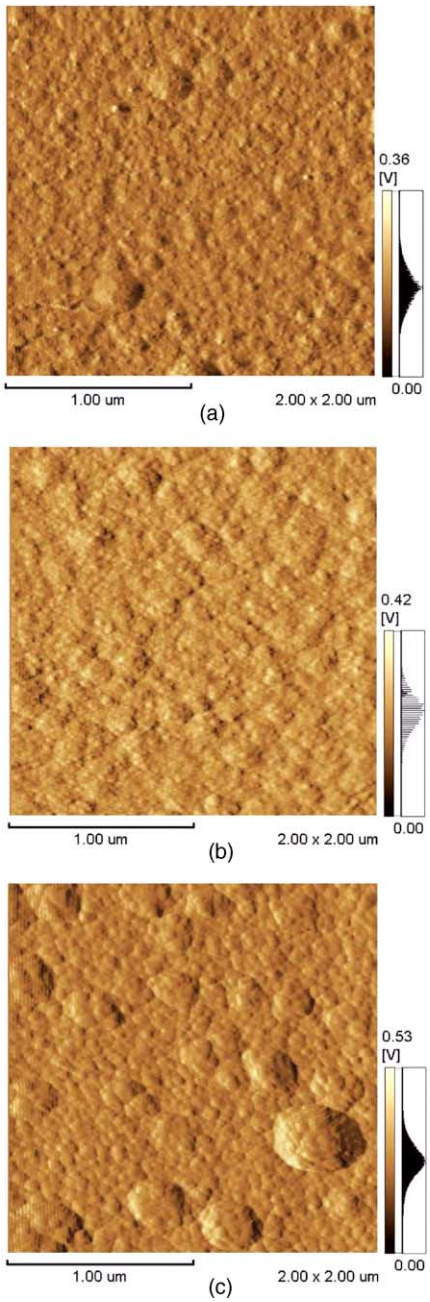

Fig. 3. FFM images of (a) TiC, (b) TiN, (c) TiCN thin films.

increased and the TiC film exhibited a higher hardness than the TiCN and the TiN films.

Young's modulus for TiC, TiN and TiCN thin films are shown in Fig. 7. The results showed that the

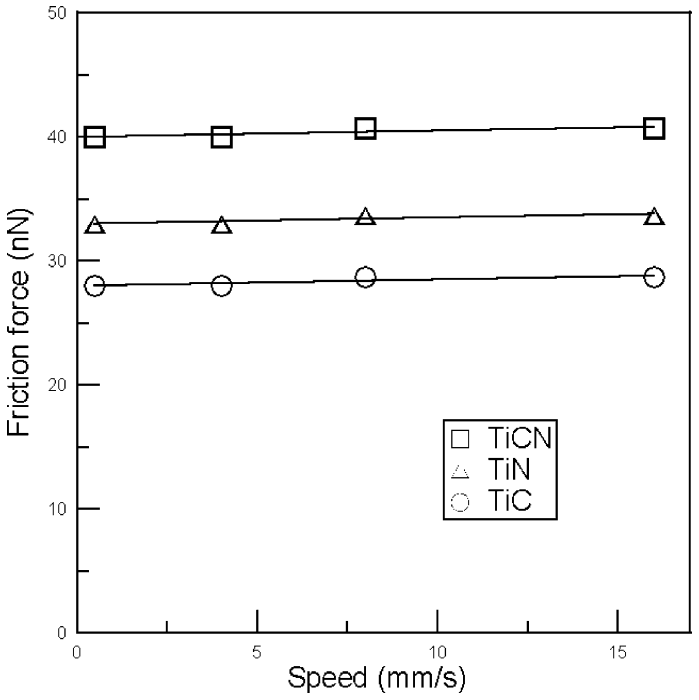

Fig. 4. The relationship of the friction force at various friction speeds.

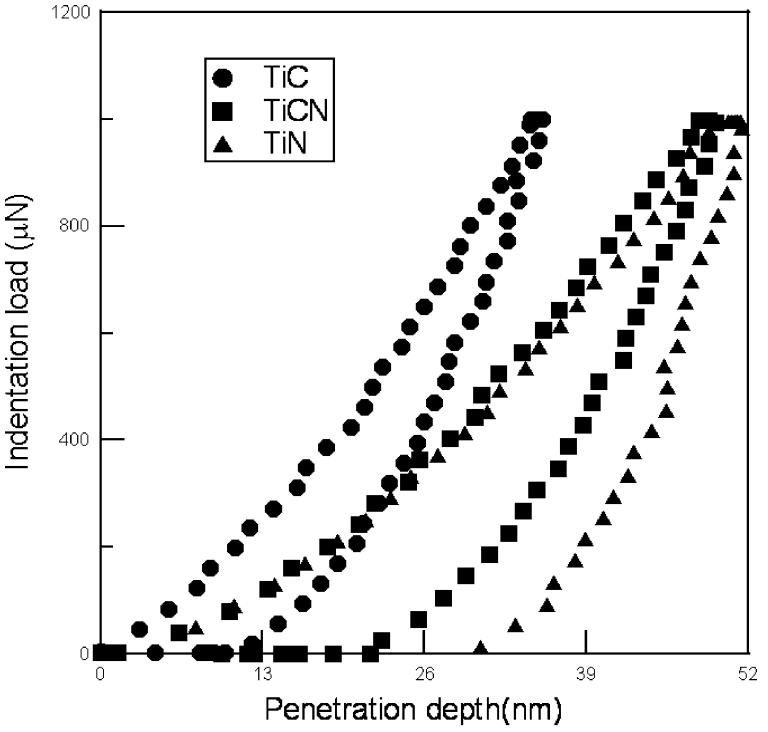

Fig. 5. Load–displacement curves of TiC, TiCN and TiN at an indentation load of 1000 μN.

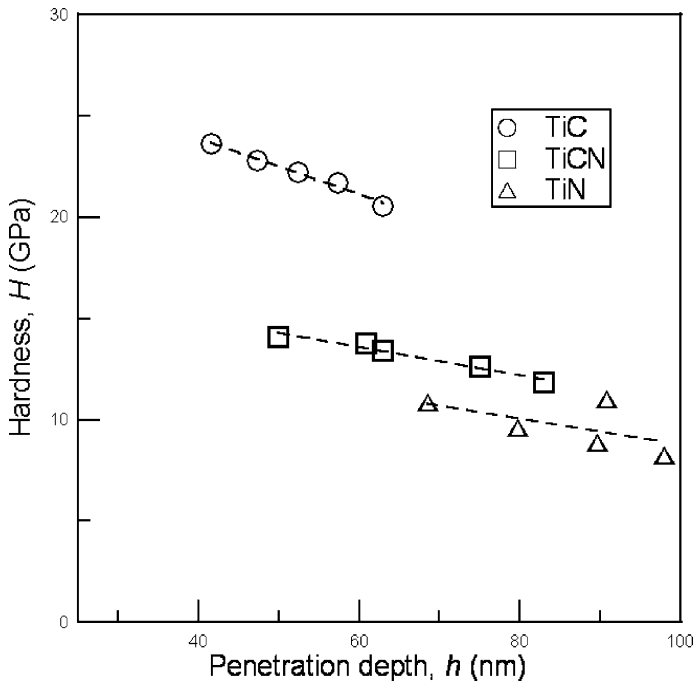

Fig. 6. Hardness of deposited films measured as a function of the penetration depth.

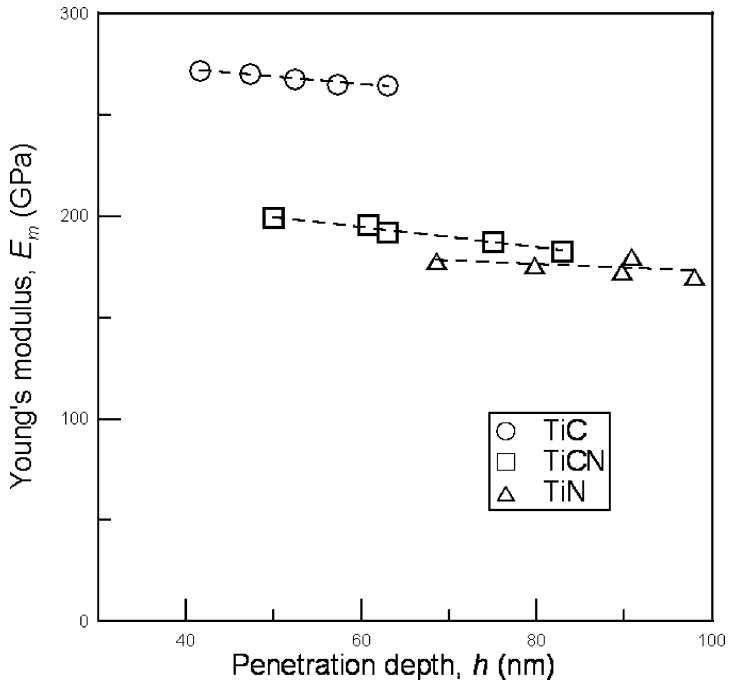

Fig. 7. Young's modulus of deposited films measured as a function of the penetration depth.

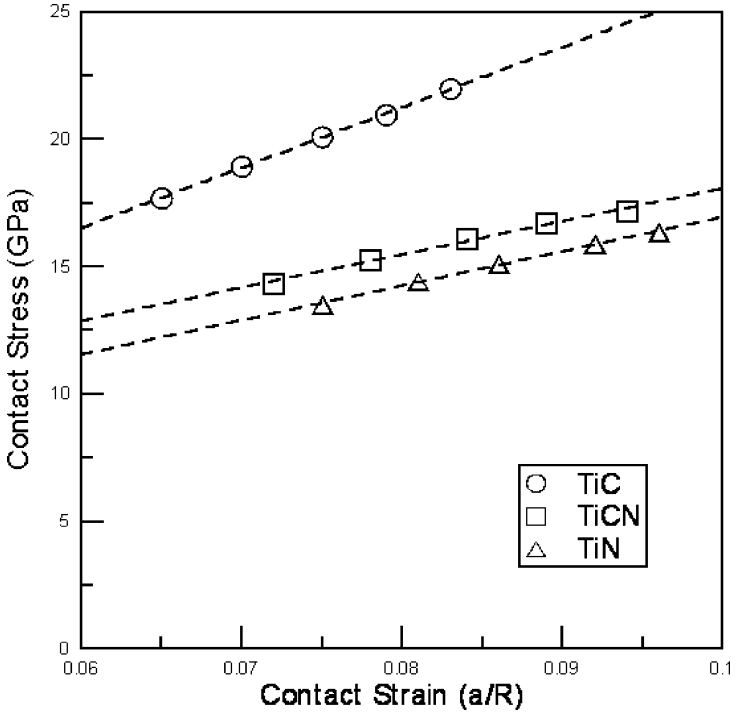

Fig. 8. Contact stress–strain relationship of TiC, TiN and TiCN thin films.

Young's moduli for TiC, TiN and TiCN thin films ranged from 264.81 to 272.06 GPa, 182.83 to 199.28 GPa and 170.34 to 180.25 GPa, respectively. The TiC film exhibits higher Young's moduli than those of the TiCN and the TiN films.

To understand the deformation mechanisms under micro-Newton level loads, the radius, a, of the contact area is calculated by using the Hertzian equation [19],

$$a = \left(\frac{3PR}{4E_r}\right)^{1/3} \quad (2)$$

where R is the radius of indenter and P is the normal load. The contact strain is defined as a/R. The relationship between stress and strain is then deduced from the above-calculations and shown in Fig. 8. The greater the stress the greater the strain and therefore the deformation of the thin films that subsequently leads to yielding behavior. As can be seen, TiC films have a lower strain than TiCN and TiN films when the indentation loads were increased.

4. Conclusion

In this study, the SPM and the nanoindentation technique were carried out for TiC, TiN and TiCN thin films deposited on silicon (1 0 0) substrate using the PECVD method to investigate their microstructures and nanomechanical properties. Results showed that the TiC films have smaller grain size, lower surface roughness and fractal dimension than the TiN and the TiCN films. The results also showed that Young's modulus and hardness both decreased when the indentation penetration depths for all specimens was increased. Harnesses for TiC, TiCN and TiN films ranged from 20.56 to 23.64 GPa, 11.84 to 14.09 GPa and 8.24 to 11.02 GPa, respectively and their Young's moduli ranged from 264.81 to 272.06 GPa, 182.83 to 199.28 GPa and 170.34 to 180.25 GPa, respectively. The contact stress–strain relationship depicts that TiC film can bear larger indentation loads and have a lower surface strain on a nanometer-scale via nanoindentation.

Acknowledgements

This work was partially supported by the National Science Council of Taiwan, under Grant Nos. NSC91-2218-E218-001 and NSC91-2212-E-218-007.

References

[1] B.E. Jacobson, C.V. Deshpandey, H.J. Doerr, A.A. Karim, R.F. Bunshah, Thin Solid Films 118 (1984) 285.
[2] I. Petror, L. Hultman, J.E. Sundgren, J.E. Greene, J. Vac. Sci. Technol. A 10 (1992) 256.
[3] S.Q. Wang, L.H. Allen, J. Appl. Phys. 79 (1996) 2446.
[4] H.M. Gabriel, K.H. Kloos, Thin Solid Films 118 (1984) 243.
[5] X.D. Li, B. Bhushan, Thin Solid Films 398 (2001) 313.
[6] N.R. Moody, W.W. Gerberich, N. Burnham, S.P. Baker, Fundamentals of Nanoindentation and Nanotribology, Materials Research Society, Warrendale, PA, 1998.
[7] S.A. Catledge, J. Bortham, Y.K. Vohra, W.R. Lacefield, J.E. Lemons, J. Appl. Phys. 91 (2002) 5347.
[8] R. Navamathavan, D. Arivuoli, G. Attolini, C. Pelosi, Appl. Surf. Sci. 180 (2001) 119.
[9] F. Arrando, M.C. Polo, P. Molera, J. Esteve, Surf. Coat. Technol. 68/69 (1994) 536.
[10] T. Deng, M. Braun, Surf. Coat. Technol. 70 (1994) 49.
[11] K.T. Rie, A. Gebauer, J. Wöhle, Surf. Coat. Technol. 86/87 (1996) 498.
[12] H.L. Wang, J.L. He, M.H. Hon, Wear 169 (1993) 195.
[13] I. Pollini, A. Mosser, J.C. Parlebas, Phys. Rep. 355 (2001) 1.
[14] N. Almgvist, Surf. Sci. 355 (1996) 221.
[15] B. Bhushan, Handbook of Micro/Nanotribology, CRC Press, New York, 1995.
[16] X. Li, B. Bhushan, Wear 220 (1998) 51.
[17] J. Ruan, B. Bhushan, ASME, J. Tribol. 116 (1994) 378.
[18] J. Ruan, B. Bhushan, J. Appl. Phys. 76 (1994) 8117.
[19] K.L. Johnson, Contact Mechanics, Cambridge University Press, Cambridge, 1985.